SuMag: Suspended Magnetometer Survey for Mineral Data Acquisition with Vertical Take-off and Landing Fixed-wing Aircraft

Robel Efrem[•◇], Alex Coutu[◇], Sajad Saeedi[•†]

***Abstract*—Multirotor Uncrewed Aerial Vehicle (UAV)s have recently become an important instrument for the magnetic method for mineral exploration (MMME), enabling more effective and accurate geological investigations. This paper explores the difficulties in mounting high-sensitivity sensors on a UAV platform, including electromagnetic interference, payload dynamics, and maintaining stable sensor performance while in flight. It is highlighted how the specific solutions provided to deal with these problems have the potential to alter the collection of data using the MMME, assisted by UAVs. The work also shows experimental findings that demonstrate the creative potential of these solutions in UAV-based data collection for the MMME, leading to improvements in effective mineral exploration through careful design, testing, and assessment of these systems. These innovations resulted in a platform that is quickly deployable in remote areas and able to operate more efficiently compared to traditional crewed aircraft or multirotor UAVs while still producing equal or higher quality results. This allows for much higher efficiency and lower operating costs for high production UAV-based data collection for the MMME.**

I. Introduction

The urgent need for efficient mineral exploration is a driving force in the global economy. The traditional ground-based methods, e.g., magnetic method for mineral exploration (MMME), are hampered by labor intensity, time consumption, and environmental restrictions. Using UAVs enables rapid coverage of large and remote areas; however, existing methods predominantly use multi-rotor vehicles, resulting in limited flight time. This paper introduces an innovative solution to these limitations: the use of UAV based Vertical takeoff and landing (VTOL) Fixed Wing (FW) systems for MMME. This approach not only accelerates the process but also reaches terrains that are otherwise inaccessible.

The integration of high-sensitivity sensors, i.e., magnetometers, on UAV platforms for mineral exploration presents unique challenges [1], including managing payload limitations, dynamics, and safety, particularly in the case of fixed-wing UAVs [2]. The most significant obstacle is minimizing Electromagnetic Interference (EMI), originating from the propulsion motor, while ensuring the suspended magnetometer systems maintain high data quality during flight [3]. These challenges stem from the complex interplay of UAV design constraints, sensor sensitivity, and the need for operational stability in varied and harsh environmental conditions [4].

Recent trends in UAV-based mineral exploration have seen a focus on VTOL fixed-wing UAVs, lauded for their increased flight endurance, flexibility, and precision [5]. However, most studies have not delved deeply into mineral sensing applications with a suspended payload or addressed the specific challenges of EMI in detail [6]. The current state-of-the-art solutions, while effective for broader applications like topographic mapping, fall short in addressing the nuanced requirements of mineral sensing, particularly in terms of EMI management and payload dynamics optimization [7]. This research aimed to bridge these gaps by enhancing VTOL UAV capabilities for mineral exploration. We focus on reducing electromagnetic interference in suspended magnetometer setups (See Fig. 1) and maintaining an acceptable level of data quality.

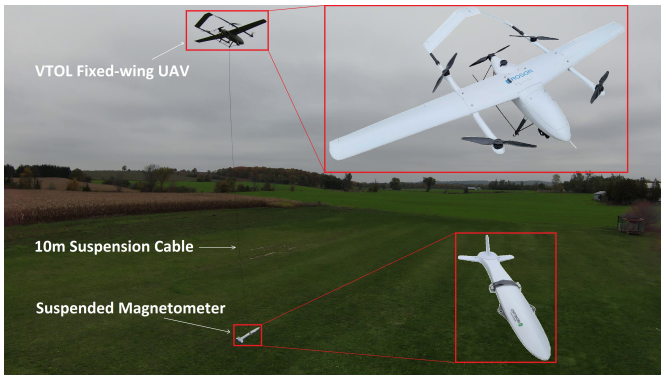

Fig. 1: The proposed VTOL fixed-wing UAV with a magnetometer in slung payload configuration, with a 10m suspension cable.

Our contributions lie in the development of a UAV platform that is not only quickly deployable and efficient but also capable of operating in challenging terrains while ensuring superior data quality and reduced operational costs. This integrated system marks a notable advancement in UAV-based MMME, setting new standards in the field. To better illustrate how this system differs compared to existing surveying systems, Table I outlines a general comparison between generic UAVs, our method (SuMag), and crewed surveying techniques. The Cost per Line Km for a Generic UAV is derived, assuming $500 in daily operating costs divided over 16 flights, each covering 22.5 km, resulting in a cost of approximately $1.38 per km. The coverage area per flight is calculated at 0.5 km² based on a 0.025 km line spacing and a 0.5-hour flight duration at 40 kmh^{-1}. Daily operating costs of $500 include fuel, maintenance, and crew, with each flight lasting 90 seconds per km at a speed of 40 kmh^{-1}. Adjustments in parameters like flight speed can modify these costs accordingly. Our method is cost-effective and of higher quality, as evidenced by the experiments. Compared to generic UAVs, our method reduces the *Cost per Line Km* nearly by half. Compared to crewed systems, our method is significantly better in terms of *Cost per Line Km* and *line spacing*.

Next, the literature review, proposed method, experiments, and conclusions are presented in Sections II-V, respectively.

•Toronto Metropolitan University, ◇Rosor Exploration, †University College London, https://sites.google.com/view/mineral-aircraft/vtol-fixed-wing-uav

II. Literature Review

Ground magnetic surveying, a versatile and long-standing technique in geophysics, involves using a magnetometer to measure surface and subsurface magnetic fields. This method is applicable across a wide range of geoscientific studies, from detecting very shallow features such as archaeological artifacts to exploring deep crustal structures. Ground magnetic surveys are beneficial for locating metallic objects or mineral deposits and provide a cost-effective approach due to their flexibility in survey area [8]. However, they are time-consuming and pose challenges in large or difficult terrains, often necessitating high-resolution follow-up scans to accurately confirm mineral deposits. Aerial surveying, utilizing sensor-equipped aircraft, overcomes these limitations by quickly capturing magnetic mineral data over large areas. Commonly, this involves attaching a magnetometer to fixed-wing aircraft, preferred for their ability to cover vast distances quickly at high altitudes, albeit at the cost of reduced data resolution and maneuverability in complex terrains [9]. Helicopters offer an alternative with their lower altitude flight and better maneuverability, yielding higher resolution data ideal for smaller or more rugged areas, though they are generally more costly and less efficient for large-scale surveys [10]. When using a magnetometer affixed to an aircraft to collect mineral data, magnetic surveys are effective at directly identifying mineral deposits containing high concentrations of ferromagnetic materials. These surveys also offer valuable indirect insights into the mineral composition or variations within the geological structure.

The emergence of UAV for various aerial surveying represents a significant advancement [11], especially in terms of data resolution. Drones, being smaller and capable of flying at lower altitudes, are well-suited for small area surveys or those involving complex terrains [12]. While offering higher resolution data and improved safety by minimizing the need for crewed flights, drones face limitations in flight time, control range, and payload capacity [13]. The use of VTOL fixed-wing UAVs has gained attention for their potential in mineral exploration, offering notable advantages such as improved flight endurance, deployment flexibility, and precise positioning in varied terrains [14], [15]. These features are critical in tasks requiring access to remote locations and high-resolution data acquisition [16]. Despite these benefits, a gap in research is evident, as most studies lack detailed exploration of VTOL fixed-wing UAVs' specific use in mineral sensing applications. Hyperspectral imaging and LiDAR have emerged as popular choices for their detailed surface analysis and topographic mapping capabilities, enabling the differentiation of rock types and identification of geological features [17], [18], [19]. The combination of multiple sensors, such as hyperspectral with magnetic sensors or LiDAR with multispectral imaging, has further expanded the UAVs' capabilities in mineral detection [20], [21]. Fixed-wing UAVs are often preferred in mineral sensing for their extended flight times and higher payload capacities, whereas multirotor UAVs offer better maneuverability at lower airspeeds [22], [23]. However, the choice between different UAV platforms depends on specific mission requirements.

While UAV-based magnetic sensing presents numerous advantages, challenges remain in signal-to-noise ratio, resolution, calibration, data fusion [24], [25], localization [26], [27], [28], [29], real-time mapping [30], and payload swing [31], [32] especially when employing hyperspectral and LiDAR sensors [33], [34]. Additionally, integrating multiple sensors on a single UAV platform poses difficulties in data interpretation and fusion [35]. Further, magnetic maps can also be used for aerial localization [36], [37], in case GPS is not available or fused with GPS for a better localization. Finally, the regulatory landscape also plays a significant, with varying legal frameworks across jurisdictions [38].

The current literature underscores the potential of VTOL fixed-wing UAVs in magnetic sensing and beyond [39], highlighting the need for further research into their application-specific optimization. Future studies should also focus on comparing operational costs, maintenance requirements, and environmental impacts of these UAV systems. Understanding these aspects will be crucial in developing more specialized and efficient UAV-based solutions for mineral exploration.

Metric	Generic UAV	Our UAV	FW (crewed)	Helicopter (crewed)
Cost of Aircraft ($)	20,000	17,000	1.5m	2.1m
Flight Duration (hrs)	0.5	3	6	3
Human Safety $\in$ (1-10)	10	10	8	7
Coverage Area/Flight (km^2)	0.5	5.9	60	15
Typical line spacing (m)	50	50	100	100
Cost per Line Km ($/km)	1.38	0.78	5.00	10.00
Flight Time (s/km)	90	45	18	35
Avg. Operating Costs ($/day)	500	500	8,000	12,000

TABLE I: General comparison between various UAVs, ours, crewed FW, and crewed helicopter for mineral sensing. Highlighted areas indicating the favorable value for each category. Platform comparison specifications are taken from that of a DJI m300, our custom VTOL FW UAV, a Piper PA-31 Navajo, and a Bell 206 JetRanger respectively.

III. Proposed Method

Here we will present our method, focusing on tackling electromagnetic interference and payload dynamics.

A. Sensor Integration

To effectively integrate a suspended magnetometer payload to a VTOL fixed-wing aircraft, first, an examination of the optimal tether length must be conducted, which would minimize EMI interference while maintaining safe operation. In this case, the main source of the EMI is produced by the high current forward propulsion motor and its accompanying electronic speed controller onboard the aircraft. The tether plays a crucial role in minimizing EMI interference between the UAV and the magnetometer sensor. An example image of what the system should look like is shown in Fig. 1.

B. Optimization of Tether Length and EMI Testing

A series of experiments were conducted to determine the optimal tether length for the suspension system. These tests

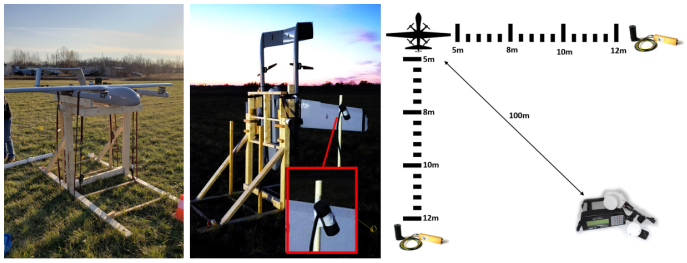

Fig. 2: (left) VTOL aircraft mounted to EMI measurement frame, (middle) the same VTOL aircraft is reoriented nose down to capture the magnetic field data in a separate axis. The magnetometer sensor is enlarged and highlighted in red on a stand to the right of the aircraft, mounted to a wooden lattice structure (shown in the picture on the middle). (right) Diagram of how the sensors were placed with respect to the vehicle for EMI testing. The GSMP-35U Potassium Magnetometer (top right and bottom left) was placed between 5-12m from the vehicle, and the GSM-19 Overhauser magnetometer (bottom right) was placed 100m away as a neutral reference.

involved strapping the full system with the propellers inverted to a frame secured to the ground, then running the electric propulsion system at different levels with a ground-based magnetic sensor recording the noise levels. All of the testing was performed at dusk when the diurnal variations caused by the Sun's magnetic field and solar wind are at their lowest [40]. A photograph of the setup is shown in Fig. 2 (left and middle). A ground magnetometer was also placed 100m away from the testing site, as well as from any roadways or power lines, to provide a reference for the testing data in case of any geomagnetic storms that might cause false positives in the data. The main magnetic sensor was placed in different areas with respect to the UAV, as well as at different distances. The tests were repeated once again with the UAV oriented vertically and spinning the motors at different RPMs to ensure a wide variety of points in 3d space relative to the UAV were recorded. A diagram of the testing procedure is shown in Fig. 2-(right).

After processing the results, the noise emitted from the main rear-mounted propulsion motor for the fixed-wing configuration was detectable only up to about 9 meters at full throttle. Due to the EMI noise spectrum following the inverse square law, the intensity of the EMI signal is inversely proportional to the square of the distance from the source, and the intensities recorded corroborate this notion [41], [42]. The motor used for testing was a T-motor AT7224 40CC, which can output approximately 17kg of thrust while drawing 6kw of power at peak thrust, to sustain flight; however, only about 1.5kw is typically required [43]. Regardless of the power level, at 10 meters distance from the UAV, there is virtually no discernible difference to the magnetic readings while the UAV is at full power or shut down. Using the data gathered from these tests, the signal-to-noise ratio of the system at 10m can be determined as ten times the logarithm base ten of the ratio of the mean signal to the standard deviation [44] (See Table II).

Parameter	Sensor Characteristic	Recorded Value
Maximum Intensity	120,000 nT	53,617.4 nT
Minimum Intensity	15,000 nT	53,612.8 nT
Mean Intensity	–	53,614.4 nT
Standard Deviation	–	0.403 nT
Number of Data Points per Test	–	100
Resolution	0.0001 nT	0.1 nT
Absolute Accuracy	0.1 nT	0.1 nT
SNR	–	102.47

TABLE II: Statistics table for magnetometer performance at 10m from an operating UAV using a GSMP35U magnetometer [45]. Maximum and minimum intensity are in reference to the full range throughout testing while the mean and standard deviation are based on 10 seconds of data while the system is at full throttle.

C. UAV and Magnetometer Modifications

Adapting the fixed-wing VTOL UAV platform with a suspended magnetometer payload required structural and functional modifications; these changes included:

1) Airframe Reinforcement: Strengthening the airframe to withstand forces exerted by the suspended payload during various flight conditions.
2) Payload Mounting Point: Integration of a large carbon fiber plate with a U-bolt at the center of gravity of the aircraft.
3) Safeguard Mechanism for Propeller: Implementation of a cage-like mechanism to prevent tether entanglement in the UAV's forward flight propeller during transition phases and flight.
4) Aerodynamic and Propulsion Adjustments: Modifications to the UAV's aerodynamics and propulsion system to support the suspended payload, maintaining flight stability and efficiency.
5) Specialized Payload Mounting Brackets: Design of non-ferrous mounting brackets to securely attach the payload to the tether.
6) Aerodynamic Payload Cover: Development of an aerodynamic cover for the payload, featuring an empennage for self-stabilization during high-speed flights.

To begin with, the airframe needed to be reinforced to withstand the forces exerted by the suspended payload during various flight conditions. The mounting point of the suspended payload was connected to a large carbon fiber plate intended to spread the load along the fuselage while still centering the force at the center of gravity. It is crucial that a slug payload is mounted at the center of gravity of a fixed-wing platform to ensure disturbances in the payload do not cause attitude alterations while in flight. Additionally, a safeguard mechanism was implemented that prevented the tether from getting entangled in the UAV's propellers during the transition, while in flight, and during de-transition.

To properly estimate the required cable length for the suspended payload from a dynamics perspective, a mathematical relation needs to be formulated taking into account all of the necessary attributes of the system. The intent is to design a system that when flown produces a suspended payload system with the least possible amount of swing as well as settling time. This is described next. The equation is a simplified model and does not account for several factors such as aerodynamic effects, wind conditions, and complex interactions between the drone and payload. A more precise estimation of the system can be achieved using processes such as computational fluid dynamics simulations to validate and refine the model, but instead, practical experiments will be completed based on the mathematical output.

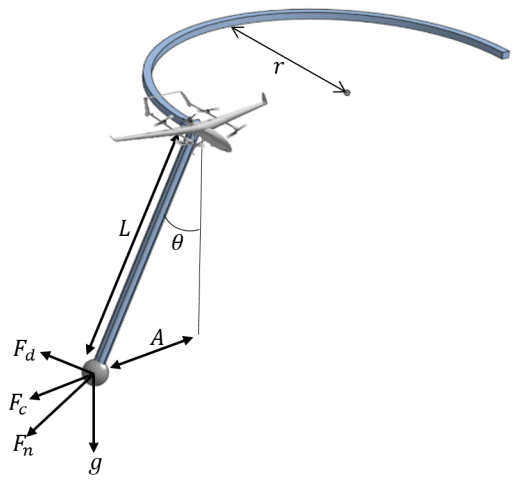

Fig. 3: Free body diagram representing the payload dynamics of the system, the point at the base representing the payload and the curve representing the path of the UAV

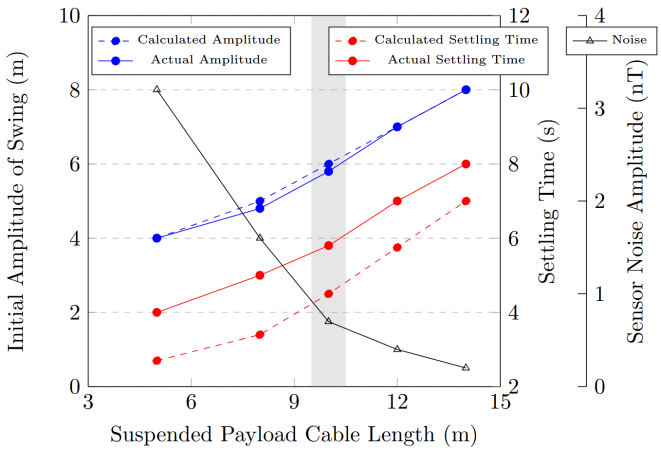

Fig. 4: Payload Dynamics Comparison: Calculated vs. Actual vs. Sensor Noise. The Grey zone indicates the configuration with the best compromise between payload dynamics and sensor noise. The difference in actual and calculated settling times could be due to model simplifications.

D. Cable Length for Suspended Payload

To develop an appropriate relation to represent this system, first, the system variables and descriptions must be outlined. Referring to the diagram shown in Fig. 3, these variables are described as follows:
A: the amplitude of the swing (m).
m_p: the mass of the payload (kg).
V: the speed of the vehicle (ms^{-1}).
r: the radius of the turn (m).
g: the gravitational acceleration $(ms^{-2}$, typically 9.81 $ms^{-2})$.
L: the length of the rope (m).
ζ: the damping ratio of the rope material (dimensionless).
C_d: the drag coefficient of the payload (dimensionless).
A_p: the cross-sectional area of the payload (m^2).
ρ: the density of air (kgm^{-3}).

As shown in Eq. (1), the algorithm can be formulated by first calculating the centrifugal force (F_c) on the payload during the turn. Then calculate the change in the angle (θ) of the rope due to the centrifugal force as well as an aerodynamic drag on the payload (F_d), and finally the net force (F_n) on the payload due to the three forces [42]:

$$F_c = \frac{m_p V^2}{r},\ \theta = \arctan\frac{F_c}{m_p g},\ F_d = \tfrac{1}{2}\rho C_d A_p V^2,$$

$$F_n = \sqrt{F_c^2 + (m_p g)^2 + F_d^2}. \tag{1}$$

The natural frequency (ω_n) of the payload swing and the damping coefficient (c) of the rope can be calculated based on the system specifications [42], shown below:

$$\omega_n = \sqrt{\frac{g}{L}},\ c = 2m_p\zeta\omega_n. \tag{2}$$

The amplitude of the swing (A) can then be estimated using an approximation for a damped harmonic oscillator. After substituting in all the necessary variables, we have the final equation for amplitude of swing from a suspended payload system of a fixed-wing UAV shown in Eq. (3):

$$A \approx \frac{F_n/m_p}{\sqrt{(\omega_n^2 - (V^2/r^2))^2 + \left(\frac{cV}{m_p r}\right)^2}} \tag{3}$$

To calculate the settling time, the effective damping coefficient (c_{eff}) must first be established, considering both the inherent damping and the damping due to drag shown in Eq. (4). The settling time (T_s) for the payload can be approximated by using the settling time equation for an underdamped harmonic oscillator. With (A) in this case being the initial amplitude from the above equation and (A_{final}) being the final amplitude within which the oscillation must remain (Eq. (4)):

$$c_{\text{eff}} = c + \frac{1}{2}\rho C_d A_p V,\quad T_s \approx \frac{\ln\left(\frac{A}{A_{\text{final}}}\right)}{\frac{c_{\text{eff}}}{2m_p}\omega_n}. \tag{4}$$

The payload swing amplitude and settling time are plotted to determine if the expected system can perform favorably at the EMI limit of 10m. The best compromise between payload swing amplitude, settling time, and EMI will be selected as the final system suspension length after testing (See Fig. 4). With a 10-meter cable length selected as the target, the next stage of testing involves performing a full systems test magnetic survey with a suspended magnetometer to prove the data is usable. Various other lengths, including 8m and 12m were tested in controlled environments using a VTOL FW UAV platform. This testing not only verifies that the suspended payload system will work to produce a high-quality magnetic dataset, but also which cable length provides the best mix between low EMI noise and acceptable payload dynamics. As the payload swings beneath the UAV in forward flight, this introduces a new mechanical noise into the system where the payload is taking measurements a few meters off from where it should be producing a lower-quality dataset. As the cable length increases, the frequency of the payload

swing decreases while the period and amplitude increase. In a pendulum, the amplitude would decrease with an increase in length, but in this case, the swing is caused primarily by the initial turn at the start and end of each flight line.

Measuring the amplitude and settling time of the suspended payload under the UAV was achieved through the use of the UAV's onboard camera. The camera, aimed at the payload, captured visual data of the payload's movements, and post-processing of this data allowed for the evaluation of payload dynamics. The amplitude, or maximum swing of the payload, was determined by identifying the furthest points of the payload's swing in the captured footage and measuring the pixel distance between them. This pixel distance was converted into the actual distance by using the known measurements of the payload size. The settling time was calculated by identifying the point in the video where the payload starts swinging (caused by initial turns at the start and end of each flight line) and the point where the swing amplitude falls within an acceptable range. The time difference between these two points is the settling time.

With a long cable, the payload swings much higher, causing the initial amplitude to be greater; this, coupled with a longer settling time, produces unfavorable results for magnetic sensing. The acquired data was analyzed for all types of noise levels, considering the impact of EMI and aerodynamic stability. After comparing the results, the 10m cable length was identified as the most suitable tether length that maintained a safe distance between the UAV and the payload, ensuring minimal EMI and payload swing.

IV. Results

After determining the optimal system characteristics, a comparative analysis needs to be run to verify if the system can acquire usable data. We compare two data sets: one from a fixed-wing crewed survey, with rear mounted stinger magnetometer, using Cs-3 cesium vapour magnetometers on the Piper Navajo PA 31-325 CR platform conducted in 2013, and the other using a proprietary magnetometer, Geometrics MagArrow, on a VTOL fixed-wing UAV platform (ours); these experiments are referred to as **Piper** and **SuMag** – Suspended Magnetometer – respectively. The analysis revealed that both systems performed similarly in terms of signal strength and signal attenuation, with a positive correlation of about 98% (signal ratio of 0.98). However, elevation changes had a lesser impact on our systems' signal strength, indicating more stability in varying terrain. The economic aspects were already summarized in Table I, favouring our system.

For the comparative analysis, an appropriately mineral-rich area was selected, and a comprehensive analysis was conducted over a field size of 500m $\times$ 700m grids in the Minden area, located in the south of Ontario, Canada. The survey was flown at 85m altitude above ground level and followed a flight pattern with a line spacing of 25m, distinctly narrower compared to traditional helicopter-borne aeromagnetic surveys, which generally utilize a line spacing of 100m shown in Fig. 6. The mission plan was generated automatically using custom-made software that outputs an

Fig. 5: (left) VTOL Fixed-wing UAV (SuMag; Suspended Magnetometer) with towed bird style magnetometer, in this case, a Geometrics MagArrow, and (right) fixed-wing crewed aircraft (Piper) with rear mounted stinger magnetometer, image from [47].

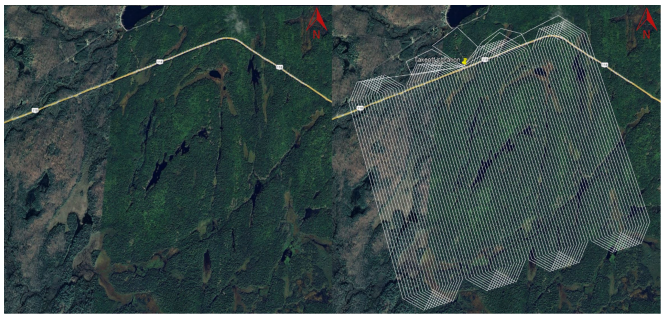

Fig. 6: (left) Image of the Minden survey site location, and (right) the same area with the four waypoint mission files overlaid on the area in white. The takeoff location has also been marked on the map. Each magnetic survey mission file is roughly 60 km and would be completed in 40 minutes.

optimized mission file based on the survey area. These files are optimized in such a way as to minimize the total number of non-production kilometers that the system needs to fly to maximize hourly in-line kilometers production. The flight plans are created using a modification of the classic boustrophedon method flight planning following a skip segment approach [46]. By skipping multiple lines this optimization reduces the amount of swing.

After performing a set of flights to compare the data of each system, the noise analysis revealed that the systems are similar in terms of high-frequency noise. To compensate for differences in line spacing between the two datasets, the Piper data was resampled to approximate our system's data sampling intervals. Overall, while both systems showed comparable performance in signal strength and attenuation as seen in Fig. 7, our UAV system resulted in higher quality data due to its lower altitude. Comparing the two Total Magnetic Field (TMF) measurement maps from two different surveys, the Piper survey depicts sharper boundaries and greater detail in color transitions compared to the fixed-wing survey in the lower altitude locations. Both maps display broadly consistent patterns of magnetic anomalies, indicating similar underlying geological structures. However, Piper's survey reveals more nuanced variations and distinct localized features, such as smaller-scale anomalies, which are not as pronounced in the fixed-wing survey. The differences in the detail and granularity of the anomalies highlight the variance in data resolution between the two survey methods. For full resolution maps, please refer to the link provided[1].

Several other analysis techniques were considered based on the specific objectives of the project and the resultant data

[1]https://sites.google.com/view/mineral-aircraft/vtol-fixed-wing-uav

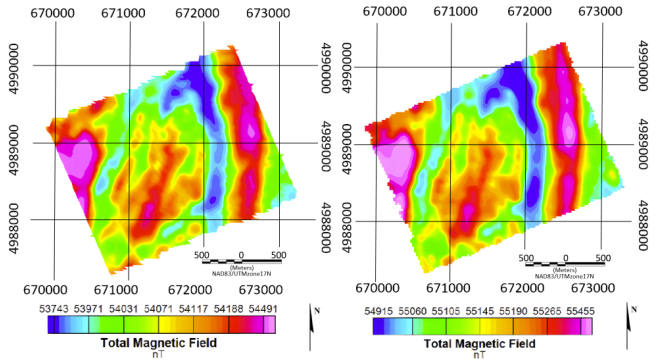

Fig. 7: (left) Fixed-wing crewed aircraft (Piper) total magnetic intensity mapped vs (right) our VTOL fixed-wing UAV (SuMag) total magnetic intensity. These two figures show that the VTOL fixed-wing survey over the same area provides equal or better resolution data compared to the crewed survey. This is achieved while being safer and more economical in comparison. Numbers surrounding the plot indicate Eastings and Northings, with the compass indicating magnetic north. See full resolution maps [48].

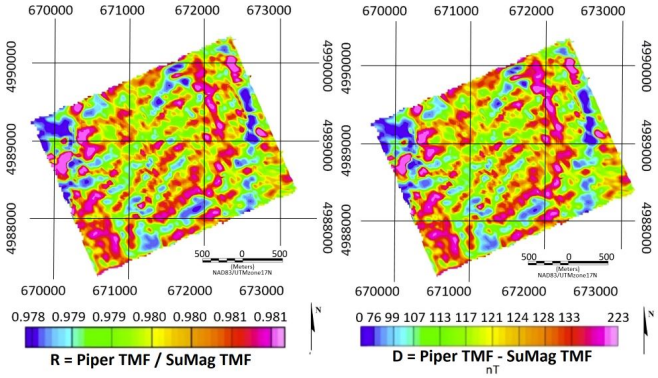

Fig. 8: (left) Ratio-based comparison of the signal strength between the crewed aircraft (Piper) system and ours, and (right) subtraction-based comparison. Piper's total magnetic frequency as a ratio compared to our system's total magnetic frequency is represented as a Nanotesla (nT) reading, and the subtraction-based method of the Piper data set minus our fixed-wing data set is outputted in nTs as well. Numbers surrounding the plot indicate Eastings and Northings. The compass indicates magnetic north. See full resolution maps [48].

quality enhancements. Radially Averaged Power Spectrum (RAPS) was considered for the analysis to better analyze the overall distribution of spectral energy in an isotropic manner across the data set. In the end, the computational cost and time associated with transforming and analyzing data in the frequency domain outweighed the benefits, especially for this specific comparison use case, where simpler spatial domain techniques will suffice. Additionally, the Reduction to the Pole (RTP) process was not included as the area has a very low magnetic latitude, which reduces the necessity of RTP, as the magnetic field in Ontario has a high magnetic inclination. Should the location have been located closer to the equator with a lower magnetic inclination, the RTP procedures may have been a necessity [49]. Additionally, the geological structure of the region is relatively simple and well-understood, diminishing the benefits of edge enhancement in further delineating geological features. These factors, combined with the survey's straightforward objectives, indicated that simpler data processing methods were sufficient to create a comparison between the two systems.

Fig. 8 reveals the signal ratio between crewed aircraft (Piper) and our fixed-wing data to be nearly 1, indicating both have similar capabilities when levelled at the same altitude. The TMF range is indicated at the bottom of the image, showing the minimum and maximum nT readings for that section of the flight. The statistical analysis of the crewed aircraft data led to a mean value of 1082 nT and a zero offset value of 116 nT, which was added to the Piper total magnetic intensity vs our fixed-wing total magnetic intensity difference to convert it into positive values for easier comparison. Normalization and calibration in data analysis, while beneficial, come with potential downsides such as the loss of absolute reference, potential misinterpretation, and the amplification of noise. In this study, meticulous steps were implemented to address these challenges and to minimize their effects, ensuring the results maintain both relevance and accuracy. This normalization process was required in order to properly perform the subtraction-based analysis but the unnormalized data can be found in Fig. 7. After applying these methods, results depicted in Fig. 8 confirmed that changes in signal largely stem from topographical variations, rather than differences in the acquisition systems' capabilities.

Shuttle Radar Topography Mission (SRTM) was a collaborative project to generate high-resolution digital topographic maps of the Earth's surface that depict the height of the Earth's landforms above sea level. The correlation between magnetic images and SRTM elevation data suggests that the observed changes in signal strength are also influenced by the area's geology. To confirm that signal change is due to terrain, a terrain profile was extracted from both grids and contrasted with the observed difference between the two systems' signals. Fig. 9 shows the location of the chosen profile and the variations in signal strength between the two systems in relation to SRTM-derived elevations. Both systems have equivalent signal measurement when leveled at the same altitude. This leveling process involves using the upward continuation method to simulate the effect of measuring it from a higher altitude than originally recorded. This technique smooths out local anomalies and reduces noise, making it easier to compare datasets collected at different altitudes or with varying resolutions. This process was applied to our UAV data to make the datasets more comparable, enhancing the analysis between different survey methods. Though the data was re-leveld, distinctive variations occur in valleys and hills. Our system performs better in low-elevation areas, with only subtle differences detected from the Piper's dataset. In high-elevation areas, the difference nears zero, mainly because both systems are close to the magnetic source, and the fixed-wing easily maintains terrain clearance. The average variation in the calculated signal strength difference is around 60 nT to 80 nT, the typical range of an Overhauser magnetometer is from 20,000 to 100,000 nT for reference. Over larger distances, both systems show minor variations with subtle topography changes, with the UAV system being higher resolution at lower altitudes.

V. Conclusions and Future Works

This research provided insight into the challenges and solutions associated with integrating high-sensitivity sensors

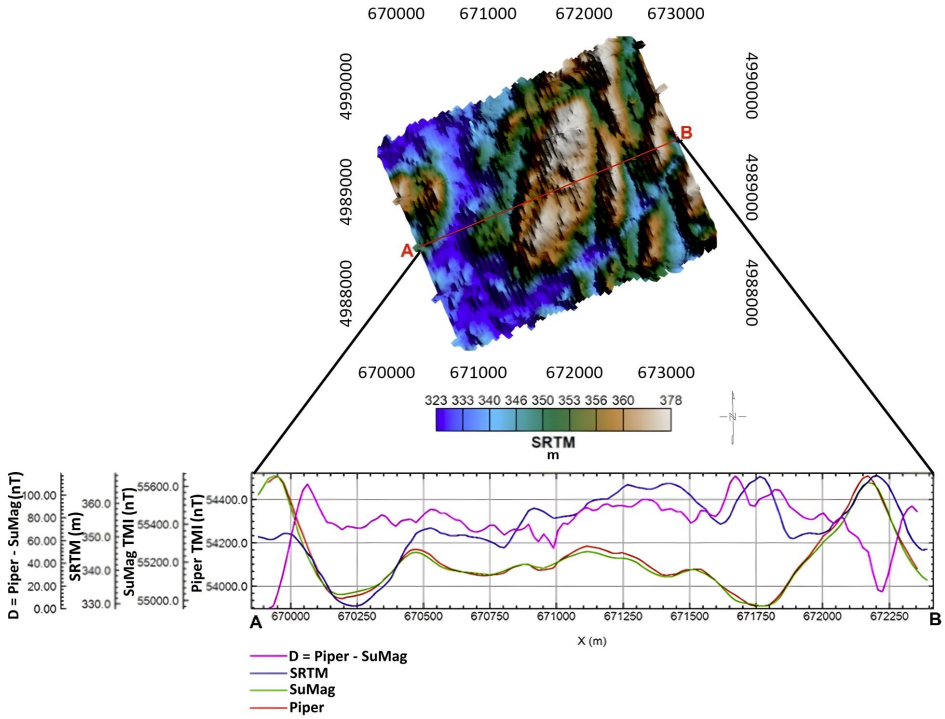

Fig. 9: Graphing the observed relationship of variation in signal strength to the SRTM. The Piper minus SuMag (D = Piper-SuMag) plot indicates the difference in nT between the two readings, displaying higher performance in areas with lower elevation. The individual Total Magnetic Intensity (TMI) of both sensors (in nT) are also plotted alongside the SRTM elevation (in m). Numbers surrounding the plot indicate Eastings and Northings.

onto VTOL UAVs. Our novel approach to sensor integration on VTOL UAVs, addressed challenges like electromagnetic interference and payload dynamics, which have been barriers in the past. The results have shown the potential of the proposed solution in the field of UAV-based data acquisition.

In the future, we will explore the possibility of deploying multiple UAVs to make the mineral exploration more automated and economically viable [50], [51]. It is also possible to transport the sensor [52] with multiple smaller UAVs. Parallelly, the rich amount of data we accumulate from VTOL UAVs points towards the necessity of 3D data fusion techniques and analysis. The rapidly expanding fields of machine learning and artificial intelligence offer enticing prospects, potentially generating models tailor-made for deciphering magnetic mineral data from VTOL UAVs. Also, as we push the boundaries of VTOL UAV capabilities, safety and regulatory considerations must remain at the forefront, necessitating research into robust safety protocols and alignment with contemporary aviation regulations [53].

ACKNOWLEDGEMENT(S)

This work was supported by Mitacs grant number IT36710.

REFERENCES

[1] S. A. H. Mohsan, M. A. Khan, and Y. Y. Ghadi, "Editorial on the advances, innovations and applications of UAV technology for remote sensing," *Remote Sensing*, vol. 15, p. 5087, 2023.

[2] G. M. Vangu, "The use of drones in mining operations," *Mining Revue*, vol. 28, no. 3, pp. 73–82, 2022.

[3] H. Shahsavani, "An aeromagnetic survey carried out using a rotary-wing UAV equipped with a low-cost magneto-inductive sensor," *International Journal of Remote Sensing*, vol. 42, no. 23, pp. 8805–8818, 2021.

[4] C. Leech, S. Burns, and K. Hurley, "Acquisition challenges for high quality data using a UAV deployed magnetometer," in *Sixth International Conference on Engineering Geophysics*, Virtual, 2021, oct. 25–28, 2021.

[5] O. Tziavou, S. Pytharouli, and J. Souter, "Unmanned Aerial Vehicle (UAV) based mapping in engineering geological surveys: Considerations for optimum results," *Engineering Geology*, vol. 232, pp. 12–21, 2018.

[6] N. Lu, Y. Xi, H. Zheng, W. Gao, Y. Li, Y. Liu, Z. Cui, G. Liao, and J. Liu, "Development of a hybrid fixed-wing UAV aeromagnetic survey system and an application study in chating deposit," *Minerals*, vol. 13, p. 1094, 2023.

[7] D. Giordan, M. S. Adams, I. Aicardi, M. Alicandro, P. Allasia, M. Baldo, P. De Berardinis, D. Dominici, D. Godone, P. Hobbs, V. Lechner, T. Niedzielski, M. Piras, M. Rotilio, R. Salvini, V. Segor, B. Sotier, and F. Troilo, "The use of Unmanned Aerial Vehicles (UAVs) for engineering geology applications," *Bulletin of Engineering Geology and the Environment*, vol. 79, no. 7, pp. 3437–3481, 2020.

[8] G. Vitale, S. Scudero, A. D'Alessandro, A. Pisciotta, R. Martorana, and P. Capizzi, "New ultraportable data logger to perform magnetic surveys," in *2019 International Symposium on Advanced Electrical and Communication Technologies (ISAECT)*, 2019.

[9] M. Mat, "Magnetic surveys: Principles, applications & geology science," https://geologyscience.com/geology-branches/geophysics/magnetic-surveys/, 2023, accessed on: Dec. 3, 2023.

[10] M. G. Persova, Y. G. Soloveichik, D. V. Vagin, D. S. Kiselev, A. P. Sivenkova, and E. I. Simon, "Resolution analysis of airborne electromagnetic survey using helicopter platform and UAV," in *2021 XV International Scientific-Technical Conference on Actual Problems Of Electronic Instrument Engineering (APEIE)*, Novosibirsk, Russian Federation, 2021, pp. 591–594.

[11] C. Gao, F. Daxinger, L. Roth, F. Maffra, P. Beardsley, M. Chli, and L. Teixeira, "Aerial image-based inter-day registration for precision agriculture," in *IEEE International Conference on Robotics and Automation*, 2024.

[12] D. Jiang, Z. Zeng, S. Zhou, Y. Guan, and T. Lin, "Integration of

an aeromagnetic measurement system based on an Unmanned Aerial Vehicle platform and its application in the exploration of the ma'anshan magnetite deposit," *IEEE Access*, vol. 8, pp. 189 576–189 586, 2020.
[13] S. Greengard, "When drones fly," *Communications of the ACM*, vol. 62, no. 11, pp. 16–18, 2019.
[14] F. Nex and F. Remondino, "UAV for 3d mapping applications: A review," *Applied Geomatics*, vol. 6, no. 1, pp. 1–15, 2014.
[15] M. Akshat, S. Jayachandran, S. Kenche, A. Katoch, A. Suresh, E. Gundabattini, S. K. Selvaraj, and A. A. Legesse, "A review on vertical take-off and landing (VTOL) tilt-rotor and tilt wing Unmanned Aerial Vehicles (UAVs)," *Journal of Engineering*, p. 1803638, 2022.
[16] L. Pádua, J. Vanko, J. Hruška, T. Adão, J. J. Sousa, E. Peres, and R. Morais, "UAS, sensors, and data processing in agroforestry: A review towards practical applications," *International Journal of Remote Sensing*, vol. 38, no. 8–10, pp. 2349–2391, 2017.
[17] I. F. Barton, M. J. Gabriel, J. Lyons-Baral *et al.*, "Extending geometallurgy to the mine scale with hyperspectral imaging: a pilot study using drone- and ground-based scanning," *Mining, Metallurgy & Exploration*, vol. 38, pp. 799–818, 2021.
[18] U. Niethammer, M. R. James, S. Rothmund, J. Travelletti, and M. Joswig, "UAV-based remote sensing of the super-sauze landslide: Evaluation and results," *Engineering Geology*, vol. 128, pp. 2–11, 2012.
[19] R. Salvini, S. Riccucci, D. Gullì, R. Giovannini, C. Vanneschi, and M. Francioni, "Geological application of UAV photogrammetry and terrestrial laser scanning in marble quarrying (apuan alps, italy)," in *Engineering Geology for Society and Territory - Volume 5*, G. Lollino, A. Manconi, F. Guzzetti, M. Culshaw, P. Bobrowsky, and F. Luino, Eds. Springer, 2015, pp. 1883–1887.
[20] R. Jackisch, Y. Madriz, R. Zimmermann, M. Pirttijärvi, A. Saartenoja, B. H. Heincke, H. Salmirinne, J.-P. Kujasalo, L. Andreani, and R. Gloaguen, "Drone-borne hyperspectral and magnetic data integration: Otanmäki Fe-Ti-V deposit in finland," *Remote Sensing*, vol. 11, no. 18, p. 2084, 2019.
[21] Y. Shendryk, J. Sofonia, R. Garrard, Y. Rist, D. Skocaj, and P. Thorburn, "Fine-scale prediction of biomass and leaf nitrogen content in sugarcane using UAV lidar and multispectral imaging," *Intl J. of Applied Earth Observation and Geoinformation*, vol. 92, p. 102177, 2020.
[22] O. Dundar, M. Bilici, and T. Unler, "Design and performance analyses of a fixed wing battery VTOL UAV," *Engineering Science and Technology, an International Journal*, vol. 23, no. 5, pp. 1182–1193, 2020.
[23] J. Shahmoradi, E. Talebi, P. Roghanchi, and M. Hassanalian, "A comprehensive review of applications of drone technology in the mining industry," *Drones*, vol. 4, no. 3, p. 34, 2020.
[24] E. Le Grand and S. Thrun, "3-axis magnetic field mapping and fusion for indoor localization," in *IEEE International Conference on Multisensor Fusion and Integration for Intelligent Systems*, 2012, pp. 358–364.
[25] J. Moore and R. Tedrake, "Magnetic localization for perching uavs on powerlines," in *2011 IEEE/RSJ International Conference on Intelligent Robots and Systems*, 2011, pp. 2700–2707.
[26] N. Akai and K. Ozaki, "Gaussian processes for magnetic map-based localization in large-scale indoor environments," in *IEEE/RSJ IROS*, 2015, pp. 4459–4464.
[27] M. Deshpande, M. Majji, and J. H. Ramos, "Magnetic field aided vehicle localization with acceleration correction," in *IEEE/RSJ IROS*, 2024, pp. 3234–3239.
[28] M. Turan, Y. Almalioglu, E. P. Ornek, H. Araujo, M. F. Yanik, and M. Sitti, "Magnetic- visual sensor fusion-based dense 3d reconstruction and localization for endoscopic capsule robots," in *2018 IEEE/RSJ International Conference on Intelligent Robots and Systems (IROS)*, 2018, pp. 1283–1289.
[29] H. Yim, H. Kang, T. D. Nguyen, and H. R. Choi, "Electromagnetic field tof sensor fusion for advanced perceptual capability of robots," *IEEE RAL*, vol. 9, no. 5, pp. 4846–4853, 2024.
[30] S. Saeedi, B. Bodin, H. Wagstaff, A. Nisbet, L. Nardi, J. Mawer, N. Melot, O. Palomar, E. Vespa, T. Spink, C. Gorgovan, A. Webb, J. Clarkson, E. Tomusk, T. Debrunner, K. Kaszyk, P. Gonzalez-De-Aledo, A. Rodchenko, G. Riley, C. Kotselidis, B. Franke, M. F. O'Boyle, A. J. Davison, P. H. J. Kelly, M. Luján, and S. Furber, "Navigating the landscape for real-time localization and mapping for robotics and virtual and augmented reality," *Proceedings of the IEEE*, vol. 106, no. 11, pp. 2020–2039, 2018.
[31] A. Faust, I. Palunko, P. Cruz, R. Fierro, and L. Tapia, "Learning swing-free trajectories for uavs with a suspended load," in *IEEE International Conference on Robotics and Automation (ICRA)*, 2013, pp. 4902–4909.
[32] I. Palunko, R. Fierro, and P. Cruz, "Trajectory generation for swing-free maneuvers of a quadrotor with suspended payload: A dynamic programming approach," in *IEEE International Conference on Robotics and Automation (ICRA)*, 2012, pp. 2691–2697.
[33] A. F. Goetz, "Three decades of hyperspectral remote sensing of the earth: A personal view," *Remote Sensing of Environment*, vol. 113, pp. S5–S16, 2009.
[34] G. Vosselman, B. Gorte, G. Sithole, and T. Rabbani, "Recognising structure in laser scanner point clouds," in *International Archives of the Photogrammetry, Remote Sensing and Spatial Information Sciences*, vol. 46, 2013, pp. 33–38.
[35] S. T. Thiele, S. Lorenz, M. Kirsch, I. C. C. Acosta, L. Tusa, E. Herrmann, R. Möckel, and R. Gloaguen, "Multi-scale, multi-sensor data integration for automated 3-d geological mapping," *Ore Geology Reviews*, vol. 136, p. 104252, 2021.
[36] N. Metni, J.-M. Pflimlin, T. Hamel, and P. Soueres, "Attitude and gyro bias estimation for a flying uav," in *IEEE/RSJ International Conference on Intelligent Robots and Systems (IROS)*, 2005, pp. 1114–1120.
[37] Y.-J. Ryoo, E.-S. Kim, Y.-C. Lim, and J.-S. Lee, "Design of magnet based position sensing system for autonomous vehicle robot," in *IEEE/RSJ International Conference on Intelligent Robots and Systems (IROS)*, 2004, pp. 2378–2383 vol.3.
[38] A. Molnar and C. Parsons, "Unmanned Aerial Vehicles (UAVs) and law enforcement in australia and canada: Governance through 'privacy' in an era of counter-law?" in *National Security, Surveillance and Terror*, R. Lippert, K. Walby, I. Warren, and D. Palmer, Eds. Palgrave Macmillan, 2016, pp. 183–200.
[39] C. Le Gentil, M. Vayugundla, R. Giubilato, W. Stürzl, T. Vidal-Calleja, and R. Triebel, "Gaussian process gradient maps for loop-closure detection in unstructured planetary environments," in *IEEE/RSJ International Conference on Intelligent Robots and Systems*, 2020, pp. 1895–1902.
[40] G. D. Egbert, P. Alken, A. Maute, and H. Zhang, "Modelling diurnal variation magnetic fields due to ionospheric currents," *Geophysical Journal International*, vol. 225, no. 2, pp. 1086–1109, 2020.
[41] (2014) Inverse Square Law. Accessed: 3-Jan-2014. [Online]. Available: http://hyperphysics.phy-astr.gsu.edu/hbase/Forces/isq.html
[42] D. Halliday, R. Resnick, and J. Walker, *Fundamentals of Physics*, 12nd ed. John Wiley & Sons, Inc., 2021.
[43] T-Motor. T-Motor Drone Motor Propeller. https://store.tmotor.com/goods-1094-AT7224+40CC.html.
[44] F. F. Mazda, *Telecommunications Engineer's Reference Book*. Focal Press, 1998, ch. 10, pp. Chapter 10 – Signals and Noise.
[45] Gem Systems, "UAV Sensors Components," https://www.gemsys.ca/uav-magnetometers/, Gem Systems Advanced Magnetometers, 2024, accessed: insert-date-here.
[46] G. Fevgas, T. Lagkas, V. Argyriou, and P. Sarigiannidis, "Coverage path planning methods focusing on energy efficient and cooperative strategies for unmanned aerial vehicles," *Sensors*, vol. 22, no. 3, p. 1235, 2022.
[47] M. Willems. (2009, July 12) C-GJBG: Piper PA-31-310 Navajo C: Goldak airborne surveys: Matt Willems. https://www.jetphotos.com/photo/6611557.
[48] R. Efrem, A. Coutu, and S. Saeedi. (2025, July 31) SuMag UAV. https://sites.google.com/view/mineral-aircraft/vtol-fixed-wing-uav.
[49] S. S. Ganguli and S. K. Pal, "Gravity-magnetic appraisal of the southern part of the Cauvery Basin, eastern continental margin of India (ECMI): Evidence of a volcanic rifted margin," *Frontiers in Earth Science*, vol. 11, 2023.
[50] S. Saeedi, M. Trentini, M. Seto, and H. Li, "Multiple-robot simultaneous localization and mapping: A review," *Journal of Field Robotics*, vol. 33, no. 1, pp. 3–46, 2016.
[51] R. Murai, J. Ortiz, S. Saeedi, P. H. J. Kelly, and A. J. Davison, "A robot web for distributed many-device localization," *IEEE Transactions on Robotics*, vol. 40, pp. 121–138, 2024.
[52] H. A. Jaafar, C.-H. Kao, and S. Saeedi, "MR.CAP: Multi-robot joint control and planning for object transport," *IEEE Control Systems Letters*, vol. 8, pp. 139–144, 2024.
[53] J. Saunders, S. Saeedi, and W. Li, "Autonomous aerial robotics for package delivery: A technical review," *Journal of Field Robotics*, vol. 41, no. 1, pp. 3–49, 2024.